

See discussions, stats, and author profiles for this publication at: <https://www.researchgate.net/publication/281564614>

Modeling hydrologic response to climate change and shrinking glaciers in the highly glacierized Kunma Like River catchment, Central Tian Shan Mountains

Article in *Journal of Hydrometeorology* · August 2015

DOI: 10.1175/JHM-D-14-0231.1

CITATIONS

14

READS

375

9 authors, including:



Qiudong Zhao

Chinese Academy of Sciences

31 PUBLICATIONS 217 CITATIONS

[SEE PROFILE](#)



Shiqiang Zhang

Northwest University

67 PUBLICATIONS 695 CITATIONS

[SEE PROFILE](#)



Haidong Han

Chinese Academy of Sciences

55 PUBLICATIONS 853 CITATIONS

[SEE PROFILE](#)



Xu Junli

Chinese Academy of Sciences

37 PUBLICATIONS 613 CITATIONS

[SEE PROFILE](#)

Some of the authors of this publication are also working on these related projects:



Study on the ice volume changes of several glacier centers in the exterior basins of Tibetan Plateau [View project](#)



Hydrometeorological Observation and Study in High Altitude Area [View project](#)

Modeling Hydrologic Response to Climate Change and Shrinking Glaciers in the Highly Glacierized Kunma Like River Catchment, Central Tian Shan

QIUDONG ZHAO,^{*,+} SHIQIANG ZHANG,[#] YONG JIAN DING,^{*} JIAN WANG,⁺ HAIDONG HAN,⁺ JUNLI XU,^{*} CHUANCHENG ZHAO,⁺ WANQIN GUO,^{*} AND DONGHUI SHANGGUAN^{*}

** State Key Laboratory of Cryospheric Sciences, Cold and Arid Regions Environmental and Engineering Research Institute, Chinese Academy of Sciences, Lanzhou, China*

+ Division of Hydrology and Water–Land Resource in Cold and Arid Regions, Cold and Arid Regions Environmental and Engineering Research Institute, Chinese Academy of Sciences, Lanzhou, China

College of Urban and Environmental Science, Northwest University, Xian, China

(Manuscript received 12 December 2014, in final form 28 July 2015)

ABSTRACT

Arid and semiarid lowland areas of central Asia are largely dependent on fluvial water originating from the Tian Shan. Mountain glaciers contribute significantly to runoff, particularly in summer. With global warming, the total glacier area in the Kunma Like River catchment declined by 13.2% during 1990–2007. For future water resources, it is essential to quantify the responses of hydrologic processes to both climate change and shrinking glaciers in glacierized catchments, such as the headwaters of the Tarim River. Thus, a degree-day glacier melt algorithm was integrated into the macroscale hydrologic Variable Infiltration Capacity model (VIC). Good results were obtained for monthly runoff simulations in the Kunma Like River catchment, which suggest that the extended VIC has acceptable performance. Because of increased precipitation and air temperature, annual runoff in the catchment has increased by about $4.07 \times 10^8 \text{ m}^3 \text{ decade}^{-1}$ during 1984/85–2006/07. Under the assumption of the same climatic conditions, sensitivity analyses indicated that annual and summer river runoff volumes would decrease by 9.3% and 10.4%, respectively, for reductions in glacier area of 13.2%. The variation coefficient of annual runoff also increased because of shrinking glaciers. Runoff scenarios for warmer future climate and various deglaciation situations suggest that reductions in glacier area by >30% will likely produce less meltwater in summer and river runoff will decline. Consequently, the annual total discharge of the Kunma Like River is projected to decrease by 2.8%–19.4% in the 2050s scenario because of glacier shrinking.

1. Introduction

The Tian Shan, one of the largest mountain systems in central Asia, stretches 2000 km from west to east and lies between 39° and 46°N and 69° and 95°E. Based on remote sensing data, it has been established that across the entire mountain area, which ranges in elevation from 2800 to 7400 m MSL, there are 15 953 glaciers that cover 15 416 km² (Liu 1995; Shi 2008). Glaciers are major sources of water in central Asian endorheic basins,

supplying water to approximately 50 million people in Kyrgyzstan, Kazakhstan, Uzbekistan, northern Tajikistan, and Xinjiang and supporting the lowland agriculture, urban areas, and industry within these regions (Aizen et al. 2006; Singh et al. 2011).

Glaciers are sensitive indicators of climate change. Glaciers in many parts of the world are in rapid retreat because of global warming, and the glaciers of the Tian Shan have been exhibiting similar trends. From field surveys and remote sensing data, many studies (e.g., Aizen et al. 2006; Liu et al. 2006; Bolch 2007; Shangguan et al. 2009; Narama et al. 2010; Wang et al. 2011) have suggested that glacier area in the Tian Shan has decreased by more than 10% since the 1970s, and this decrease has been connected to the increase in summer temperatures. It is inevitable that the shrinking glaciers will affect the runoff in the glacier-fed watersheds of the Tian Shan in

Corresponding author address: Yong Jian Ding, State Key Laboratory of Cryospheric Sciences, Cold and Arid Regions Environmental and Engineering Research Institute, Chinese Academy of Sciences, 320 Donggang West Road, Lanzhou, China 730000, China.
E-mail: dyj@lzb.ac.cn

terms of quantity and seasonal distribution (Hagg et al. 2007; Sorg et al. 2012). In the short term, the glacier runoff has increased because of the ample quantities of water supplied by retreating glaciers. However, continuing loss of glacier mass will gradually reduce both glacier-fed and total runoff (Braun et al. 2000; Hock 2005; Hagg et al. 2007; Zhao et al. 2013). This loss will eventually transform glacial–nival runoff regimes into nival–pluvial regimes, which will generate much greater interannual variability of water yield (Malone 2010; Sorg et al. 2012).

Successful models of glacier-derived runoff need to accurately simulate the formulation of melt processes. Energy-balance models and temperature-index approaches have been developed in the last few decades. Both of these approaches have been used extensively to simulate glacier melt in mountain areas (e.g., Hock 2005; Hock and Holmgren 2005; Hock et al. 2005; Gao et al. 2010; Jiang et al. 2010; Zhang et al. 2012a). The energy-balance models are based on solid physical mechanisms; however, they are often impractical because of their substantial data requirements, which cannot be met in data-scarce mountain watersheds. Temperature-index models have been used in a wide range of applications because of their minimal data requirements, reduced computational cost, and generally good performance. Thus, such models have been used frequently to calculate runoff in glacial catchments (e.g., Klok et al. 2001; Hock 2005; Huss et al. 2008; Schaefli and Huss 2011; Immerzeel et al. 2012) and have been shown to produce good agreement between the calculated and observed runoff in some glacierized catchments (Hagg et al. 2007; Gao et al. 2012).

For simulating hydrologic processes in alpine glacierized catchments, a hydrologic model should contain snow and ice and frozen soil schemes. Unfortunately, most popular large-scale models do not consider mountain glacier-related hydrologic processes and the effect of frozen soil on discharge. Thus, for catchments where these processes are relevant, it is necessary to design a hydrologic model that contains such schemes, preferably with the requirement of easily accessible observational data as input. Such a model could then be readily applied to data-scarce alpine basins.

Most research on the response of hydrologic processes in glacierized catchments to climate change (Singh and Kumar 1997; Liu et al. 2003; Chen et al. 2006; Huss et al. 2008; Piao et al. 2010; Zhao et al. 2013) have used a static glacier mask and have not taken into account the impact of glacier area changes on hydrologic processes. Only a limited number of studies have addressed glacier retreat and associated changes in runoff (e.g., Kotlyakov and Severskiy 2009; UNDP 2009; Sorg et al. 2012).

In this study, we developed a simple glacier melt (degree-day) method within the framework of the macroscale

hydrologic Variable Infiltration Capacity model (VIC) (Liang et al. 1996; Cherkauer and Lettenmaier 1999, 2003). The extended VIC was evaluated for its ability to represent glacier melt and runoff production for a glacierized catchment. In this paper, based on the combination of observed data and simulations, we analyze glacier variation and the response of hydrological processes in a typical glacierized catchment of the central Tian Shan during recent decades. We then project the potential change of the response of the hydrologic processes to future climate scenarios.

2. Description of study area

The study area of the Kunma Like River basin (one of the major tributaries of the Aksu River) is on the southern slope of central Tian Shan, and it extends westward from northwestern China into the republics of Kazakhstan and Kyrgyzstan. The Kunma Like River catchment includes the Tuomuer and Hantengeri mountain glaciers, and it is highly glacierized (25%). The catchment extends across 12 816 km² of alpine topography with elevations ranging from 1400 to 7100 m MSL (Fig. 1).

The catchment can be characterized by its vast area, complex terrain, and wide variations in regional climatic. The high-mountain zone has lower temperatures, plentiful precipitation and abundant snow and ice. The mid-mountain zone has the widest precipitation distribution and distinct spatial variations of temperature. The low-mountain zone has high temperatures, low precipitation, and strong heating. This is characteristic of typical dry continental climates, which usually exhibit negligible precipitation, abundant solar radiation, extreme heat, and intense evaporation (Tang et al. 1992; Jiang et al. 2005).

The Kunma Like is typical of rivers for which glacier and snow meltwater constitute the primary sources of water supply. The annual runoff volume is $4.87 \times 10^9 \text{ m}^3 \text{ yr}^{-1}$, measured at the Xiehela stream gauge in China. Over 70% of runoff is from snow and ice meltwater (Hu 2004; Zhao et al. 2013). Runoff is minimal during the winter months since most precipitation is stored as snow. In contrast, a great majority of the annual runoff volume (>88%) occurs during the summer melt season (May–September; Hu 2004; Shen et al. 2009; Zhao et al. 2013). Studies have clearly shown that the catchment glaciers and hydrologic processes have varied in response to global climate change (Shi et al. 2002; Jiang et al. 2005; Shangguan et al. 2009; Yu et al. 2011; Zhao et al. 2011, 2013).

3. Data and methodology

a. Model description

The glacier algorithm described in this study is intended to simulate glacier melt as a component of the

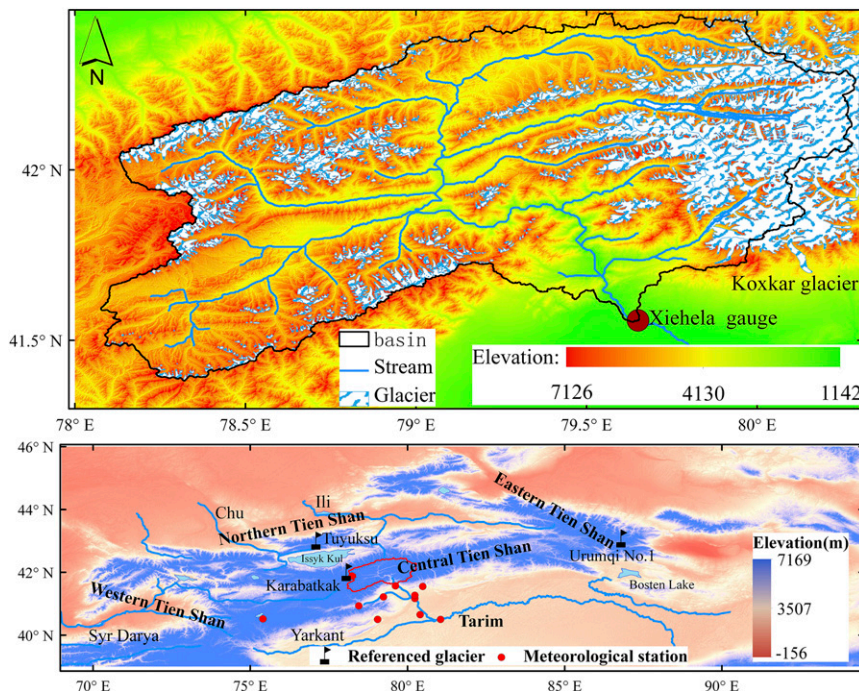


FIG. 1. Map of Kunma Like River catchment: topography, meteorological stations, and glaciers.

VIC. The water balance of the glaciers is resolved for a daily time step. The degree-day glacier melt algorithm is based on the work of Gao et al. (2010) and Zhang et al. (2012a).

1) MACROSCALE HYDROLOGICAL VIC

The VIC is an energy-balance and surface water model that was initially created for large-scale applications. It has been widely applied in many diverse environments, typically at spatial scales of $1/8^\circ$ latitude \times 2° longitude, thereby representing large continental river basins (Liang et al. 1994, 1996; Nijssen et al. 2001; Bowling et al. 2004; Costa-Cabral et al. 2008). The VIC curve describes the relationship between the infiltration capacity and the soil moisture distribution. This curve is used in the simulation of surface runoff (Liang et al. 1994). An energy and mass balance model is used to generate snowpack dynamics using two snow layers of variable thickness (Cherkauer and Lettenmaier 2003).

The effects of frozen soil on surface water and energy fluxes are represented using the method of Cherkauer and Lettenmaier (1999, 2003). A nonlinear soil moisture relationship based on empirical values was used to generate base flow (Liang et al. 1994). Surface runoff and base flow released from model grid cells are routed to the basin outlet using an independent routing model (Lohmann et al. 1998a,b). The routing model was designed for applications at large scales. All moisture

transfer between grid cells is handled via a runoff routing postprocessor, and the subsurface moisture transfer between grid cells is ignored. The VIC can accept either daily or subdaily meteorological data as input (or a combination of the two). Furthermore, the VIC has some flexibility, such that variables and their combinations can both be used. The minimum sets of variables required by the VIC are daily total precipitation (rain and/or snow), daily maximum and minimum temperatures, and daily average wind speed. In this case, the VIC uses the mountain microclimate simulation model (MTCLIM) algorithms and Tennessee Valley Authority algorithm (Thornton and Running 1999; Bras 1990; Bohn et al. 2013) to produce daily humidity, incoming short- and longwave radiation, pressure, and other parameters.

2) GLACIER SUBGRID PARAMETERIZATION SCHEME

(i) Fraction surface coverage

In addition to the vegetation and bare soil classes, a new gridcell type (glacier) was introduced into the mosaic of the VIC in order to account for mountain glaciers on a subgrid scale (Fig. 2). Most glaciers are found at higher elevation in the respective grid cells. The meteorological conditions (temperature, precipitation, and other parameters) of glaciers are substantially different from the model gridcell means. For more accurate glacier melt

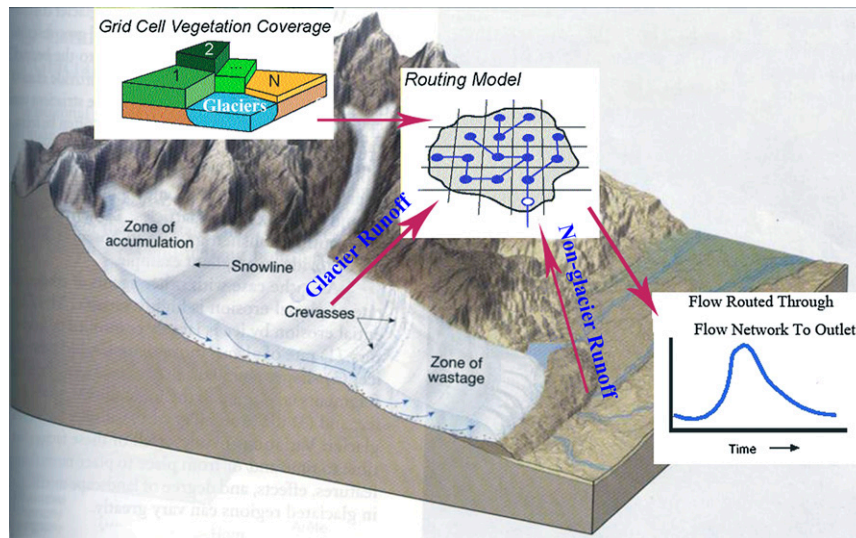


FIG. 2. Schematic representation of the VIC glacier scheme.

simulation, we partitioned glaciers into elevation bands (called glacier bands) and simulated them separately in each grid cell, referring to the method of VIC snow bands (Fig. 3). The fraction of each glacier band's area within the respective grid cell was calculated statistically from the input spatial distribution data of the glaciers. The elevation of each glacier band was derived statistically from high-resolution digital elevation model (DEM) data. The new method of representing glaciers in a model grid box is a major improvement on previous work (Zhao et al. 2011, 2013), which treated all individual glaciers within a grid box as an ice body.

(ii) Atmospheric subgrid variability

On the VIC subgrid level, glacier bands and gridcell median are expected to exhibit fundamental differences in climate forcing. Glaciers tend to form in the parts of the terrain with the lowest temperatures and highest moisture contents. In this study, each glacier band's mean elevation has been used to lapse the gridcell mean temperature and precipitation to a more accurate local estimate, according to the following:

$$T_{\text{band}} = T_0 + T_{\text{alt},m}(E_{\text{band}} - E_0) \quad \text{and} \quad (1)$$

$$P_{\text{band}} = P_0 \left[1 + \frac{P_{\text{alt},m}(E_{\text{band}} - E_0)}{P_{0,m}} \right] \\ \text{if } P_{\text{band}} < 0.0, \quad P_{\text{band}} = 0.0, \quad (2)$$

where T_{band} is the daily mean air temperature in the glacier elevation band ($^{\circ}\text{C}$), T_0 is the gridcell mean

daily temperature ($^{\circ}\text{C}$), E_{band} is the mean elevation of the glacier elevation band (m), E_0 is the gridcell mean elevation (m), $T_{\text{alt},m}$ is the corresponding monthly temperature lapse rate ($^{\circ}\text{C m}^{-1}$), P_{band} is the daily precipitation falling in the glacier elevation band (mm), P_0 and $P_{0,m}$ are the gridcell mean daily and corresponding monthly precipitation (mm), and $P_{\text{alt},m}$ is the corresponding monthly precipitation gradient (mm m^{-1}). The variables $T_{\text{alt},m}$ and $P_{\text{alt},m}$ are calculated by field observation or taken from the literature.

(iii) Degree-day melt model

Simple degree-day melt models have been used widely in a variety of studies (e.g., Hock 2003; Zhang et al. 2006, 2012b) in which available data were sparse. This is because the studies calculated melt rates based on air temperature, which can be obtained easily from observations via elevation changes associated with the air temperature lapse rate. We used the simple degree-day glacier melt model to simulate snow and ice melt and accumulation in each glacier band, as follows.

Solid precipitation and liquid precipitation are differentiated by using the dual-threshold method (Kang et al. 1999). The solid precipitation $P_{s,\text{band}}$ (mm day^{-1}) in the glacier band is calculated using Eq. (3):

$$P_{s,\text{band}} = \begin{cases} P_{\text{band}} & T_{\text{band}} < T_s \\ P_{\text{band}} \left(\frac{T_{\text{band}} - T_s}{T_l - T_s} \right) & T_l \geq T_{\text{band}} \geq T_s \\ 0 & T_{\text{band}} \geq T_l \end{cases}, \quad (3)$$

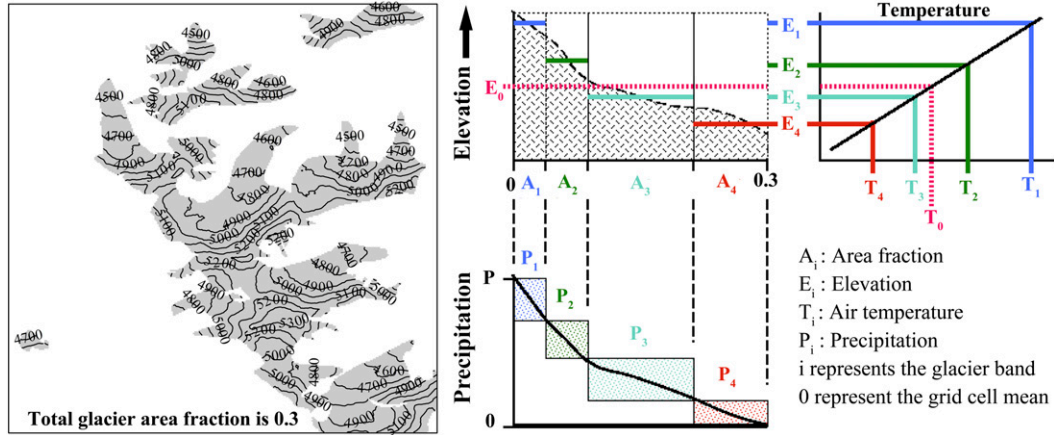


FIG. 3. Subgrid glacier parameterization for use in the VIC.

where T_l is the minimum temperature ($^{\circ}\text{C}$) that can sustain rainfall and T_s is the maximum temperature ($^{\circ}\text{C}$) at which snow can occur.

The liquid precipitation $P_{l,\text{band}}$ (mm day^{-1}) is calculated using Eq. (4):

$$P_{l,\text{band}} = P_{\text{band}} - P_{s,\text{band}} \quad (4)$$

The accumulated snow water equivalent S_{band} (mm) on the glacier surface is calculated using Eq. (5) with daily time steps ($\Delta t = 1$ day):

$$S_{\text{band}}(t) = S_{\text{band}}(t - \Delta t) + P_{s,\text{band}} \quad (5)$$

The liquid water L_{band} (mm) in the snowpack is calculated using Eq. (6):

$$L_{\text{band}}(t) = L_{\text{band}}(t - \Delta t) + P_{l,\text{band}} \quad (6)$$

When temperatures are above the threshold temperature T_T (usually 0°C), melting of snow and ice starts. The potential melting of snow $M_{p,\text{band}}(t)$ (mm) is calculated using Eq. (7):

$$M_{p,\text{band}}(t) = D_{\text{snow}}(T_{\text{band}} - T_T)\Delta t, \quad (7)$$

where D_{snow} is the degree-day factor for snow ($\text{mm } ^{\circ}\text{C}^{-1} \text{day}^{-1}$).

The variable $M_{p,\text{band}}(t)$ is then compared with the water equivalent of accumulated snow S_{band} . If $S_{\text{band}}(t)$ is greater than the $M_{p,\text{band}}(t)$, only snow that has accumulated will melt. If there is insufficient snow, ice will melt as a result of absorbing the residual positive air temperature [Eq. (8)] and the water equivalent of accumulated snow is set as zero [Eq. (9)]:

$$M_{\text{band}}(t) = \begin{cases} M_{p,\text{band}}(t) & S_{\text{band}}(t) \geq M_{p,\text{band}}(t) > 0 \\ S_{\text{band}}(t) + [M_{p,\text{band}}(t) - S_{\text{band}}(t)] \left(\frac{D_{\text{ice}}}{D_{\text{snow}}} \right) & 0 < S_{\text{band}}(t) < M_{p,\text{band}}(t), \\ D_{\text{ice}}(T_{\text{band}} - T_T) & S_{\text{band}}(t) = 0 \end{cases} \quad (8)$$

where $M_{\text{band}}(t)$ is the total melt of snow and ice (mm) and D_{ice} is the degree-day factor for ice:

$$S_{\text{band}}(t) = \begin{cases} S_{\text{band}}(t) - M_{p,\text{band}}(t) & S_{\text{band}}(t) \geq M_{p,\text{band}}(t) > 0 \\ 0 & S_{\text{band}}(t) < M_{p,\text{band}} \end{cases} \quad (9)$$

When there is accumulated snow on the ice, the snowpack will retain meltwater until the level exceeds a certain percentage (CWH; usually 10%) of the water equivalent of the snowpack. The daily runoff $R_{\text{band}}(t)$

(mm) and L_{band} in the snowpack can be calculated using Eqs. (10) and (11):

$$R_{\text{band}}(t) = L_{\text{band}}(t) + M_{\text{band}}(t) - \text{CWH}[S_{\text{band}}(t)] \quad (10)$$

if $R_{\text{band}}(t) < 0.0$, $R_{\text{band}}(t) = 0.0$ and

$$L_{\text{band}}(t) = L_{\text{band}}(t) + M_{\text{band}}(t) - R_{\text{band}}(t). \quad (11)$$

When temperatures fall below T_T , the liquid water in the snowpack will refreeze and runoff is not generated. The potential refreezing of liquid water $F_{p,\text{band}}(t)$ (mm) is calculated using Eq. (12):

$$F_{p,\text{band}}(t) = D_{\text{snow}}(\text{CFR})(T_T - T_{\text{band}})\Delta t, \quad (12)$$

where CFR is the refreezing coefficient.

The variable $F_{p,\text{band}}(t)$ is then compared with the liquid water in the snowpack. If $L_{\text{band}}(t)$ is greater than $F_{p,\text{band}}(t)$, only part of the liquid water will refreeze, whereas if there is insufficient liquid water, all the existing liquid water will refreeze and the liquid water in the snowpack is set to zero [Eq. (14)]. The refreezing of liquid water is added to the snow water equivalent on the glacier surface [Eq. (13)]:

$$S_{\text{band}}(t) = \begin{cases} S_{\text{band}}(t) + F_{p,\text{band}}(t) & L_{\text{band}}(t) \geq F_{p,\text{band}}(t) \\ S_{\text{band}}(t) + L_{\text{band}}(t) & L_{\text{band}}(t) < F_{p,\text{band}}(t) \end{cases} \quad (13)$$

and

$$L_{\text{band}}(t) = \begin{cases} L_{\text{band}}(t) - F_{p,\text{band}}(t) & L_{\text{band}}(t) \geq F_{p,\text{band}}(t) \\ 0 & L_{\text{band}}(t) < F_{p,\text{band}}(t) \end{cases}. \quad (14)$$

The glacier mass balance $B_{\text{band}}(t)$ is equal to the accumulation minus outflow runoff [Eq. (15)]:

$$B_{\text{band}}(t) = P_{\text{band}}(t) - R_{\text{band}}(t). \quad (15)$$

b. Data description

1) GLACIER AREA CHANGE DATA

The Chinese glacier inventory project group provided data on the spatial distribution of glaciers for our study catchment for three different times (1990, 2000, and 2007). These datasets are based on Landsat Thematic Mapper, Enhanced Thematic Mapper Plus, and Advanced Spaceborne Thermal Emission and Reflection Radiometer imagery. The details of the approach are provided in Liu et al. (2006), Shanguan et al. (2009), and Xu et al. (2013).

The total glacier area within the Kunma Like River catchment was 3149.4 km² in 1990, 2868.2 km² in 2000, and 2733.5 km² in 2007. The overall decrease of the glacier area was 415.9 km² (13.2%) over the entire period with a shrinkage rate of 24.46 km² yr⁻¹. The average annual glacier shrinkage was 0.89% yr⁻¹ from 1990 to 2000 and 0.67% yr⁻¹ from 2000 to 2007.

2) ATMOSPHERIC FORCING DATA

To run the VIC, the time series data of daily atmospheric factors (precipitation; wind speed; as well as maximum, minimum, and mean temperatures) from

1985 to 2007 were required. Data regarding land-cover classification and topography (elevation, vegetation, soil, and glacier presence) were also required.

There are 11 meteorological stations in and around the Kunma Like River catchment (Fig. 1). These stations vary considerably in elevation from 1012 to 3639 m. The daily air temperature data obtained at these meteorological stations were interpolated to each model grid cell (5' × 5' spatial resolution) using the broad acceptance of the gradient plus the inverse distance squared method:

$$T_0 = \left[\sum_{i=1}^n \left(\frac{1}{d_i} \right)^2 \right]^{-1} \left(\sum_{i=1}^n \left\{ [T_i + (E_0 - E_i)T_{\text{alt},m}] \left(\frac{1}{d_i} \right)^2 \right\} \right), \quad (16)$$

where T_0 is the air temperature at the predicted model grid cell (°C); T_i is the observed temperature at a neighboring weather station i (°C); d_i is the distance between weather station i and a predicted grid point; E_0 is the model gridcell mean elevation (m); E_i is the elevation of weather station i (m); $T_{\text{alt},m}$ is the temperature lapse rate (°C m⁻¹) of the corresponding month, which can be obtained from observations; and n is the number of observed neighboring stations around the model grid cell. In this paper, the nearest three stations were considered.

A gridded daily precipitation dataset (APHRODITE, version 1101R2, on 0.25° × 0.25° grids) that was created by the Asian Precipitation–Highly-Resolved Observational Data Integration Towards Evaluation of Water Resources (APHRODITE) was utilized in this study (Yatagai et al. 2012). Some studies have shown that the APHRODITE data have high correlation with data observed by rain gauges in China and exhibit good performance in depicting the amount, frequency, and intensity of precipitation (Han and Zhou 2012; Wei et al. 2013). The inverse distance squared weighting method was used to interpolate these data to a 5-min spatial resolution:

$$P_0 = \left[\sum_{i=1}^n \left(\frac{1}{d_i} \right)^2 \right]^{-1} \left\{ \sum_{i=1}^n \left[P_i \left(\frac{1}{d_i} \right)^2 \right] \right\}, \quad (17)$$

where P_0 is the daily precipitation at a predicted hydrologic model grid cell (mm); P_i is the daily precipitation at a neighboring APHRODITE precipitation dataset cell i (mm); d_i is the distance between the precipitation dataset cell i and the predicted grid point; and n is the number of neighboring APHRODITE precipitation dataset cells. In this paper, the nearest three cells were considered.

TABLE 1. Monthly precipitation gradient [mm (100 m)^{-1}] and air temperature (T_{max} , T_{min} , and T_{avg}) lapse rates [$^{\circ}\text{C (100 m)}^{-1}$] in Kunma Like River catchment.

	Jan	Feb	Mar	Apr	May	Jun	Jul	Aug	Sep	Oct	Nov	Dec
Precipitation gradient	0.12	0.14	0.55	0.64	1.33	1.28	1.18	1.23	0.87	0.40	0.26	0.22
Lapse rate T_{max}	-0.31	-0.51	-0.68	-0.80	-0.82	-0.79	-0.72	-0.70	-0.71	-0.69	-0.50	-0.30
Lapse rate T_{min}	-0.28	-0.46	-0.58	-0.60	-0.64	-0.64	-0.62	-0.60	-0.54	-0.46	-0.40	-0.32
Lapse rate T_{avg}	-0.29	-0.48	-0.64	-0.72	-0.76	-0.73	-0.68	-0.65	-0.62	-0.56	-0.42	-0.29

The inverse distance squared weighting method was also used to interpolate the daily wind speed data of the stations to each model grid cell.

3) OTHER DATA

Data on soil characteristics including soil field capacity, soil type, and saturated hydrologic conductivity were obtained from the Food and Agriculture Organization soil database (Global Soil Data Task Group 2000). This database contains the most globally consistent and detailed soil data (Webb et al. 1993). Vegetation classification and its parameters (including albedo, monthly leaf area index, and other parameters) were obtained from the 1-km global land-cover product generated by the University of Maryland (Hansen et al. 1998). The topography data were obtained from the global 30-arc-s DEMs of the Shuttle Radar Topography Mission (SRTM), version 4 (Farr et al. 2007). The SRTM DEM data were used to create input files for the routing model and to establish elevations for the glacier bands and model grid cells.

Monthly discharge data in the Kunma Like River catchment were obtained from the Xinjiang Uyghur Autonomous Region Hydrological Institute for the period from October 1985 to September 2007. These data were utilized for model analysis and calibration.

c. Model parameters

1) DISTRIBUTION OF GLACIERS IN KUNMA LIKE RIVER CATCHMENT

Based on the SRTM DEM and the digital vector of glaciers, the glacierized regions of the catchment were divided into 45 elevation bands at intervals of 100 m MSL for each model grid cell. The glacier spatial distribution data were obtained for three periods, and therefore we used glacier data from 1990, 2000, and 2007 for the simulation of water-year 1984/85–1993/94 (from 1 October 1984 to 30 September 1994), water-year 1994/95–2003/04 (from 1 October 1994 to 30 September 2004), and water-year 2004/05–2006/07 (from 1 October 2004 to 30 September 1994), respectively.

2) PRECIPITATION GRADIENT AND TEMPERATURE LAPSE RATE

The mean monthly air temperature (maximum, minimum, and mean) and precipitation data from 11 stations covering 1980–2010 in and around the Kunma Like River catchment were collected (Fig. 1). The monthly air temperature lapse rate and precipitation gradient were calculated (Table 1) using the simple linear regression between meteorological elements and elevation, which has been widely adopted by previous studies in other mountain regions (Mokhov and Akperov 2006; Blandford et al. 2008; Kattel et al. 2013). In high-altitude mountainous regions with sparse precipitation data, it is difficult to approximate the precipitation gradient. The maximum precipitation altitude is not considered in this gradient. Hence, the precipitation may not be accurate for some elevation bands.

3) DEGREE-DAY FACTORS

The degree-day model requires that two parameters (D_{snow} and D_{ice}) be determined. In the Tian Shan, the ablation zones of many glaciers are covered by supraglacial debris. The melt condition of ice under debris-covered parts is different from the condition of clean glaciers. Experimental studies have demonstrated the thickness of debris layers can affect the melting of underlying ice, with thin layers accelerating melting and thick debris layers reducing melting (Østrem 1959; Nakawo and Rana 1999; Hagg et al. 2008). Empirical relationships between the degree-day factor of underlying ice and debris layer thickness have been reported by several studies (e.g., Østrem 1959; Popovnin and Rozova 2002). However, these empirical relationships cannot be applied to a macroscale basin melt calculation of debris-covered glaciers, because the spatial distribution of debris thickness is very difficult to measure. Furthermore, the snow and ice degree-day factors have temporal and spatial variation (Zhang et al. 2005).

Long-term spatial snow and ice melt and meteorological observations have been obtained on the Koxkar Glacier, which is on the southern slope of the central Tian Shan near our study area (Fig. 1). The ablation zone of the Koxkar Glacier is covered by debris. Some studies of

the glacier have provided snow and ice degree-day factors based on these long-term observational data (e.g., Zhang et al. 2005, 2006; Han et al. 2009; Li et al. 2012). In this study, we selected a mean degree-day factor value (Table 2) for the Kunma Like River catchment based on earlier studies of the Koxkar Glacier, assuming that the glacier is representative of the average conditions of glaciers within the study catchment.

4) OTHER PARAMETERS

CFR and CWH were set to 0.1 based on the literature (Liu et al. 1996; Gao et al. 2010). The VIC contains adjustable parameters that can be optimized to reflect the prevailing conditions within specific catchments. The majority of soil and vegetation parameters can be approximated from the literature. However, some soil parameters were subject to calibration that was based on correspondence between the observed and simulated hydrographs. The parameters that were tuned most commonly during the VIC calibration were the infiltration parameter b_{infiltr} , fraction of maximum base flow (Ds), the thickness of the three soil layers th_j ($j = 1, 2, \text{ and } 3$), the fraction of maximum soil moisture content within the third layer (Ws), and the maximum baseflow velocity (Ds_{max} ; Xie and Yuan 2006; Huang and Liang 2006).

Calibration was then performed. For the objective function, which describes the match between the simulated and observed values, the Nash–Sutcliffe model efficiency coefficient (NS; Nash and Sutcliffe 1970) was selected. The correlation coefficient R^2 and the mean relative error (MRE) were also used for model evaluation:

$$NS = 1 - \frac{\sum_{t=1}^n (Q_{\text{obs},t} - Q_{s,t})^2}{\sum_{t=1}^n (Q_{\text{obs},t} - \bar{Q}_{\text{obs}})^2}, \quad (18)$$

$$R^2 = \left\{ \frac{\left[\sum_{t=1}^n (Q_{\text{obs},t} - \bar{Q}_{\text{obs}}) (Q_{s,t} - \bar{Q}_s) \right]^2}{\sqrt{\sum_{t=1}^n (Q_{\text{obs},t} - \bar{Q}_{\text{obs}})^2 \sum_{t=1}^n (Q_{s,t} - \bar{Q}_s)^2}} \right\}, \quad \text{and} \quad (19)$$

$$MRE = \frac{1}{n} \sum_{t=1}^n \frac{|Q_{\text{obs},t} - Q_{s,t}|}{Q_{\text{obs},t}}, \quad (20)$$

where $Q_{\text{obs},t}$ and $Q_{s,t}$ are the observed and simulated daily discharges at time step t , respectively, and \bar{Q}_{obs} and \bar{Q}_s are the mean of the n observed and simulated values, respectively.

The following steps were used for model calibration:

- 1) The model parameters Ds and Ds_{max} were calibrated to fit the lowest soil layer base flow.

TABLE 2. Model parameter values for Kunma Like River catchment.

Model parameter	Unit	Values
Degree-day factors (D_{snow} and D_{ice})	mm °C ⁻¹ day ⁻¹	3.0 and 5.0
Refreezing coefficient (CFR)	fraction	0.1
Water holding capacity of snow (CWH)	fraction	0.1
Thicknesses of the three soil layers (th_1 , th_2 , and th_3)	m	0.1, 0.3, and 2.7
Max velocity of base flow (Ds_{max})	mm day ⁻¹	20
Fraction of max base flow (Ds)	fraction	0.13
Fraction of max soil moisture content of the third layer (Ws)	fraction	0.6
Infiltration parameter (b_{infiltr})	—	0.3
Max temperature at which snow can fall (T_s)	°C	2.0
Min temperature at which rain can fall (T_i)	°C	-2.0

- 2) The infiltration parameter (i.e., b_{infiltr}) was tuned to agree with the observed flow maxima on rainfall days. A higher value was selected to produce increased surface runoff and reduced infiltration.
- 3) To increase the water content required to rapidly raise the nonlinear base flow, a higher value of Ws was selected. This tends to delay runoff maxima.
- 4) The thicknesses of the soil layers (th_2 and th_3) were set using estimated values. This is typically accomplished via arid regions having greater thickness and humid regions having lesser thickness.

Typical related soil parameters were used as initial values for our study basin (<http://www.hydro.washington.edu/Lettenmaier/Models/VIC/Documentation/SoilParam.shtml>). Monthly observed discharge data from October 1984 to September 1994 were used for the model calibration. The calibrated soil parameters are given in Table 2.

d. Downscaling GCM output

To analyze the response of hydrological processes to future climate change and glacier contraction, climatic data from phase 5 of the Coupled Model Intercomparison Project (CMIP5) global climate models (GCMs) under the RCP2.6 (low greenhouse gas emission), RCP4.5 (moderate greenhouse gas emission), and RCP8.5 (high greenhouse gas emission) scenarios were used (Meinshausen et al. 2011). Monthly historical and future temperature and precipitation simulations were derived from the Chinese National Climate Center based on three different GCMs: the Beijing Normal

University–Earth System Model (BNU-ESM); Geophysical Fluid Dynamics Laboratory Climate Model, version 3 (GFDL CM3); and the Norwegian Earth System Model, version 1 (intermediate resolution) (NorESM1-M). Further information and details regarding these models are available in the literature (Donner et al. 2011; Bentsen et al. 2013; Iversen et al. 2013; Liu et al. 2014).

To create input meteorological forcing datasets for the VIC, monthly variations of GCM predictions had to be downscaled to higher spatial resolution and daily datasets. Monthly GCM data were downscaled using the delta method (Pielke and Wilby 2012). First, we computed monthly changes of the temperature and precipitation variables at the GCM's grid nearest the study catchment for each GCM:

$$\Delta T_i = \bar{T}_{i,GCM:future} - \bar{T}_{i,GCM:reference} \quad \text{and} \quad (21)$$

$$\Delta P_i = \bar{P}_{i,GCM:future} / \bar{P}_{i,GCM:reference}, \quad (22)$$

where ΔT_i and ΔP_i are the monthly air temperature ($^{\circ}\text{C}$) and precipitation changes, respectively; $\bar{T}_{i,GCM:future}$ and $\bar{P}_{i,GCM:future}$ are the monthly mean air temperature ($^{\circ}\text{C}$) and precipitation (mm) in the future scenarios, respectively; and $\bar{T}_{i,GCM:reference}$ and $\bar{P}_{i,GCM:reference}$ are the monthly mean air temperature ($^{\circ}\text{C}$) and precipitation (mm) of the reference period, respectively.

The average monthly differences in precipitation and air temperature between the reference and the future scenarios of three GCMs were then disaggregated into daily values. The temporal downscaling was achieved by adding the daily temperature and adding or subtracting the observed precipitation amounts for precipitation events during the reference simulation period, such that the anticipated monthly changes were attained (Hagg et al. 2007). This procedure produced statistically downscaled daily time series for precipitation and temperature that were subsequently used to force the hydrologic model. The mean multiyear simulated results reflect the possible future discharge change.

4. Results

a. Discharge and glacier mass balance simulations

We used the data of spatial distribution of the glaciers in 1990, 2000, and 2007 to simulate the discharge and glacier mass balance of water-year 1984/85–1993/94, 1994/95–2003/04, and 2004/05–2006/07, respectively. Based on the aforementioned methods and parameters, river discharge and glacier mass balance were computed for the Kunma Like River catchment from October 1984 to September 2007.

1) DISCHARGE

Comparisons of monthly simulated and observed discharge for the validation period (from October 1994 to September 2007) and calibration period (from October 1984 to September 1994) are shown in Fig. 4. The associated statistical values are listed in Table 3.

The original VIC lacked a glacier melt scheme and for that reason systematically underestimated runoff. The original VIC exhibited poor performance; the values of NS and R^2 were always lower for the calibration and validation period (NS = 0.27, R^2 = 0.78, and MRE = 0.44 for the calibration period; and NS = 0.33, R^2 = 0.76, and MRE = 0.44 for the validation period). Model performance was greatly improved by coupling the glacier melt scheme, illustrated by the good scores obtained (NS = 0.95, R^2 = 0.96, and MRE = 0.16 for the calibration period; and NS = 0.90, R^2 = 0.92, and MRE = 0.20 for the validation period). This suggested that glacier meltwater is a vital component of the hydrologic cycle in the Kunma Like River catchment and that glacier hydrologic processes cannot be neglected in runoff simulations.

As can be seen from Fig. 4, the simulated discharge slightly underestimates the observations during the wet season. The major cause of the underestimation was likely a lack of accurate spatial precipitation, because of the sparse coverage of precipitation gauge stations in the high-mountain watershed. It also results in the slightly high value of MRE, although through the optimization of parameters. In terms of the performance of the extended VIC and coupled glacier melt scheme (see Table 3), the simulated discharge components can be used in further analyses.

2) GLACIER MASS BALANCE

Glacier mass balance in the catchment was estimated by the extended VIC. The mass balance year starts on 1 October and terminates on 30 September of the subsequent year. Figure 5 displays variations of glacier and cumulative mass balances in the catchment during 1984/85–2006/07. The mean annual mass balance of glaciers in the catchment was -525.9 mm water equivalent (w.e.), with total mass loss of 12.1 m w.e. over 1984/85–2006/07. Glacier mass loss caused the shrinkage of the overall glacier area.

There are no long-term observed data of glacier mass balance in the Kunma Like River catchment. For validating the model, a comparison of the simulated mass balance within the catchment with observations and previous studies of the Karabatkak Glacier, Tuyuksu Glacier, and Urumqi No.1 Glacier, which are

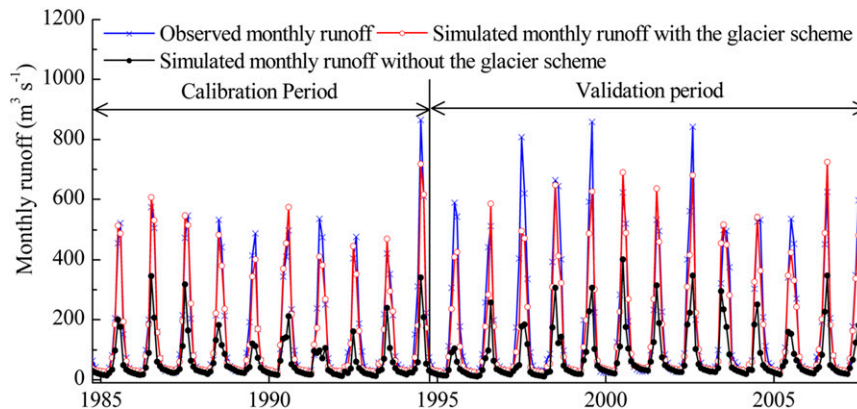


FIG. 4. Observed and simulated monthly discharge for the calibration and validation periods.

benchmark glaciers in the Tian Shan, is shown in Table 4. The comparisons show that our simulated cumulative mass balance within the Kunma Like River catchment is close to the observations of nearby glaciers. Thus, the extended VIC can efficiently simulate glacier mass balance, but with some deviations due to inaccurate precipitation data from the alpine regions.

b. Runoff and glacier mass balance response to climate change

To clarify further the effects of climate change on various discharge components for the Kunma Like River watershed, we separated the simulated discharge into glacier (including precipitation runoff over glacier areas) and nonglacier runoff. In this study, we counted the annual runoff of the water year (begins on 1 October and ends on 30 September of the following year), annual precipitation, melt-season (May–September) mean air temperature, and runoff in the catchment during 1984/85–2006/07 (Fig. 6).

Because of inaccuracies in the precipitation data, there is some disparity between observed runoff and the simulated total runoff after 1996/97. However, the rising trend of observed discharge was largely reproduced by the model. This indicates that the simulated response of annual runoff to climate change is reasonable. Here, we analyze the response of the different runoff components to climate change based on the simulated values.

The simulation results indicate that runoff from the glacierized area contributed 53.6% of the discharge during 1984/85–2006/07, consistent with the value of 52.4% from Chen et al. (2007). Nonglacier runoff showed a rising trend similar to that of precipitation at $2.99 \times 10^8 \text{ m}^3 \text{ decade}^{-1}$ (Fig. 6b). The tendency of annual glacier runoff was similar to that of mean

temperature at $1.08 \times 10^8 \text{ m}^3 \text{ decade}^{-1}$ (Fig. 6b). Because of the increasing precipitation and temperature, total annual river runoff had a significant increase of $4.07 \times 10^8 \text{ m}^3 \text{ decade}^{-1}$ (Fig. 6b). Detailed analysis revealed that enhanced nonglacier runoff was the key driver of the increase in annual total runoff; that is, 73.5% of the total increase was from nonglacier areas and only 26.5% was from intense ice melt.

As can be seen in Fig. 6b, the fluctuation of simulated total and annual observed runoff corresponds with the fluctuation of glacier runoff before 1996/97. After 1996/97, the variation of total runoff was controlled by increasing precipitation, while the amplitude of variation in glacier runoff is very small (Fig. 6). The correlation relationships between the observed annual runoff and melt-season air temperature and annual precipitation also show the runoff change and shift for two periods (Fig. 7). As seen from Fig. 7, the observed total runoff is positively correlated with melt-season air temperature and negatively correlated with precipitation during 1984/85–1996/97 (Figs. 7a,b). Conversely, the total runoff is negatively correlated with melt-season air temperature and positively correlated with precipitation during 1997/98–2006/07 (Figs. 7c,d).

A regression analysis suggested that the mass balance is significant ($p < 0.01$) and negatively correlated with glacier runoff, with a correlation coefficient of -0.87 (Figs. 5, 6b). This relationship indicates that a greater negative mass balance generates additional glacier melt. The variation of glacier mass balance is very similar to that of glacier runoff, which is mainly controlled by the melt-season air temperature. Compared with 1984/85–1996/97, the mean annual precipitation increased by 30% and the melt-season air temperature increased by 0.2°C during 1997/98–2006/07 (Fig. 6a). However, the mean glacier mass loss was 529.5 mm yr^{-1} during 1984/85–1996/97 and 521.3 mm yr^{-1} during 1997/98–2006/07. This

TABLE 3. Performance comparison summary between observed and simulated monthly runoff in Kunma Like River watershed.

	Calibration period			Validation period		
	NS	R^2	MRE	NS	R^2	MRE
Simulating using extended VIC	0.95	0.96	0.16	0.90	0.92	0.20
Simulation using previous VIC	0.27	0.78	0.44	0.33	0.76	0.44

occurred because abundant precipitation forms a thick snowpack above the ice that slows glacier melt because of the higher snow albedo and smaller degree-day factor. Although the air temperature was higher, glacier mass loss was slightly reduced during 1997/98–2006/07, which has also been reported by Zhao et al. (2011, 2013) and Pieczonka et al. (2013).

c. Impact of shrinking glacier area on discharge

For estimating the effect of the shrinking glacier area on hydrologic processes, we compared the simulated discharge during 1984/85–2006/07 using the glacier area for the three periods under the assumption of the same climatic conditions (Fig. 8). The effects on runoff were more pronounced in dry years than in wet years (Figs. 8a, 6a). Thus, sensitivity analyses of the simulated annual total discharge using the three glacier datasets could more accurately assess the hydrologic effects of shrinking glaciers on runoff.

Relative to the glacier area in 1990, areal losses of 8.9% and 13.2% were associated with annual total discharge reductions of 6.9% ($\sim 3.42 \times 10^8 \text{ m}^3 \text{ yr}^{-1}$) and 9.3% ($\sim 4.58 \times 10^8 \text{ m}^3 \text{ yr}^{-1}$), respectively. These results indicate that the effect of change of glacier area on discharge cannot be neglected in the hydrological modeling of the catchment. Figure 8b shows the seasonal distribution of monthly runoff during 1984/85–2006/07, which illustrates that the effects of shrinking glacier area on discharge during June–September

were more pronounced. This corresponds to the agricultural irrigation season in downstream regions (Li 2010). The comparative results show that the shrinkage of glacier area by 8.9% and 13.2% reduced the total river discharge during June–September by 7.7% and 10.4%, respectively, affecting agricultural activities in the arid and semiarid lowland areas. We also analyzed the impact of shrinking glacier area on nonglacier runoff and found that the effect is smaller. The annual nonglacier runoff would only increase by 2.2% following a loss of glacier area of 13.2%. The reduction in glacier runoff results in the reduction of total runoff (not shown).

Reduced glacier runoff in wet years and increased annual glacier runoff in arid years (Fig. 6) dampens interannual variation in river discharge. This is commonly referred to as the glacier compensation effect (Lang 1986; Hock et al. 2005). A smaller annual discharge variation is more beneficial to water resource management and development. We analyzed the impact of shrinking glaciers on this variation using the variation coefficient of annual runoff (Cv):

$$Cv = \frac{\sqrt{\frac{1}{n} \sum_{i=1}^n (Q_i - Q_{\text{avg}})^2}}{Q_{\text{avg}}}, \quad (23)$$

where Q_i is the annual discharge, Q_{avg} is the average annual discharge, and n is the total number of years.

During 1984/85–2006/07, the Cv of annual nonglacier runoff was 0.20, while that of annual total runoff was 0.13 (Fig. 6b). This demonstrates that the variation of annual river discharge clearly decreased with glacier coverage in excess of 5% (Ye et al. 2012). For evaluating the effects of shrinking glacier area on discharge variation, we calculated the Cv of annual runoff during 1984/85–2006/07 using the simulated annual discharge for glaciers in 1990, 2000, and 2007 (Fig. 8). The results

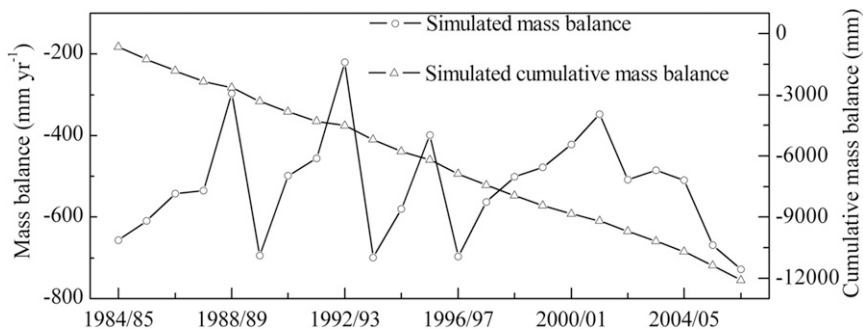


FIG. 5. Variations of annual and cumulative glacier mass balances in study catchment during 1984/85–2006/07.

TABLE 4. Comparisons of simulated mass balance in the catchment with observations from Karabatkak Glacier, Tuyuksu Glacier, and Urumqi No. 1 Glacier.

Glacier	Period	Observed mass balance (mm w.e.)	Simulated mass balance (mm w.e.)	Source
Karabatkak	1984/85–1997/98	−7327	−7445.9	Zemp et al. (2013)
Tuyuksu	1984/85–1997/98	−6984	−7445.9	Zemp et al. (2013)
Urumqi No.1	1987/88–2006/07	−9762	−10288.5	Zemp et al. (2013)

show that this C_v increased with dwindling glacier area. After glacier area losses of 8.9% and 13.2%, C_v increased by 2.4% (~ 0.004) and 3.2% (~ 0.005), respectively. Moreover, the simulation indicated that river discharge variance of the Tarim River basin headwaters increased with the loss of glacier area, which hampers agricultural activities downstream.

d. Projecting glacier and river runoffs with the 2050s scenario

Mean monthly air temperature differences (daily maximum temperature ΔT_{\max} , daily minimum temperature ΔT_{\min} , and mean temperature ΔT_{avg}) and precipitation ratios ΔP between the future scenario (2050s and from October 2044 to September 2054) and reference simulation period (from October 1984 to September 2007) for the three GCMs were calculated for the catchment. Monthly changes in temperature and precipitation under the three emission scenarios are presented in Table 5. The monthly air temperature differences and precipitation ratios between the future

scenario and reference period were finally disaggregated into model daily forcing datasets.

The extended VIC is incapable of directly describing the deglaciation processes. Therefore, the effects of climate change and glacier shrinkage on the hydrologic processes were simulated for 80%, 70%, 60%, and 50% of the 2007 glacier area and glacier area contraction from lower to higher altitudes, as described in Zhang et al. (2012a).

The seasonal distribution of monthly glacier and total river runoff responses to future climate warming (2050s) and present climate were compared for various glacier coverages (Fig. 9). Relative to the reference period (1984/85–2006/07), the air temperature will increase by over 2°C , while precipitation will increase by less than 8% by the 2050s (Table 5). Therefore, the change of total runoff will be dominated by glacier runoff (Fig. 9). The values of glacier and total runoff under the RCP8.5 scenario were greater than under the RCP4.5 and RCP2.6 scenarios, indicating that glaciers produce more meltwater under warmer climatic scenarios. By the

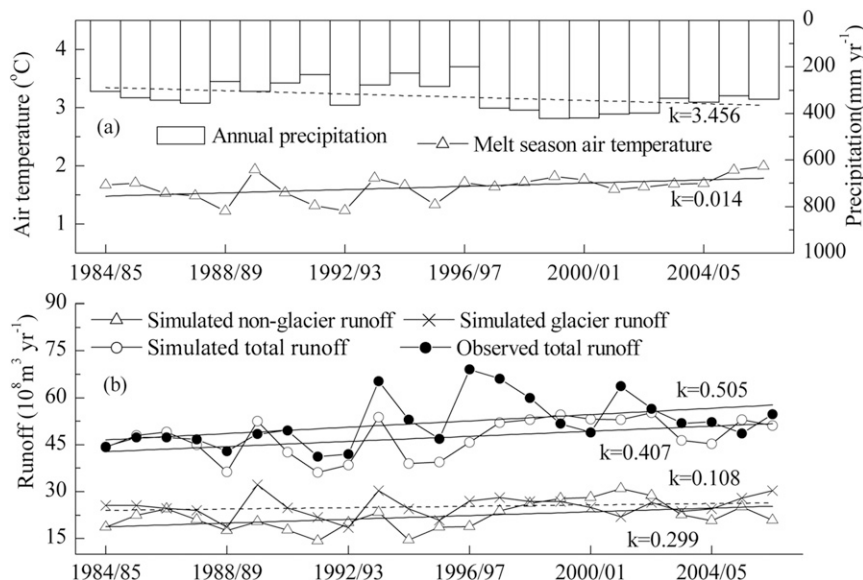


FIG. 6. Variations of melt-season (a) mean temperature and annual precipitation and (b) runoff in Kunma Like River catchment during 1984/85–2006/07. Straight lines are fitted for each variable and k is their slope ($108 \text{ m}^3 \text{ yr}^{-2}$). Solid lines indicate that the trend passed the t test ($p < 0.05$).

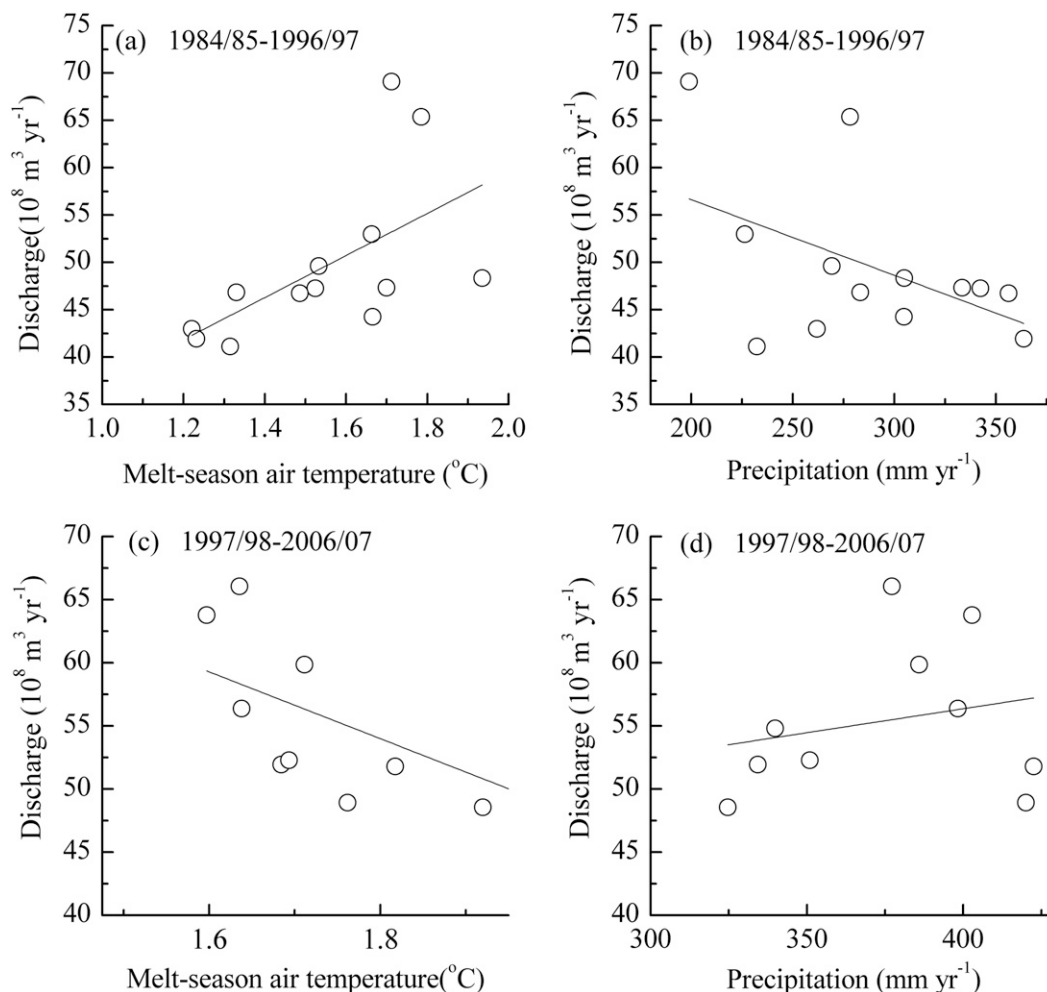


FIG. 7. Scatterplots between observed annual discharge and melt-season (a),(c) air temperature and (b),(d) annual precipitation for two periods.

2050s, if the glacier area is reduced by 20% compared with 2007, both glacier and total runoffs in the Kunma Like River basin under the three scenarios will exceed those under the present climate, because of the enhanced glacier meltwater. For a glacier area decrease of 30%, the glacier and total runoffs only show an increasing trend under the RCP8.5 scenario. Both runoffs were less than in the reference period under all three climatic scenarios for reductions of glacier area $>30\%$.

According to the current glacier shrinkage rate ($0.78\% \text{ yr}^{-1}$), the glacier area of the catchment will very likely decline by 33%–50% under the 2050s scenario because of the warmer climate, and thus the annual total runoff will also very likely decline because of the reduced level of glacier meltwater. Detailed analysis suggests that relative to the reference period, annual total discharge under the 2050s scenario will likely decrease by 2.8%–19.4%, while total discharge during summer

(June–September) will decline by 8.2%–25.1%. These results indicate that the potential change of glacier area is very important for the management of water resources downstream of the Aksu River basin.

5. Discussion

Precipitation and temperature are two of the most important climatic variables in discharge simulations. For the land surface water budget, precipitation is the most important source of water (Fekete and Vorosmarty 2004). Air temperature is obviously the main driving variable behind estimations of snow and ice melt.

In this study, precipitation products were used for discharge simulation in the large catchment where the availability of surface gauging data was insufficient. A number of precipitation products have been published,

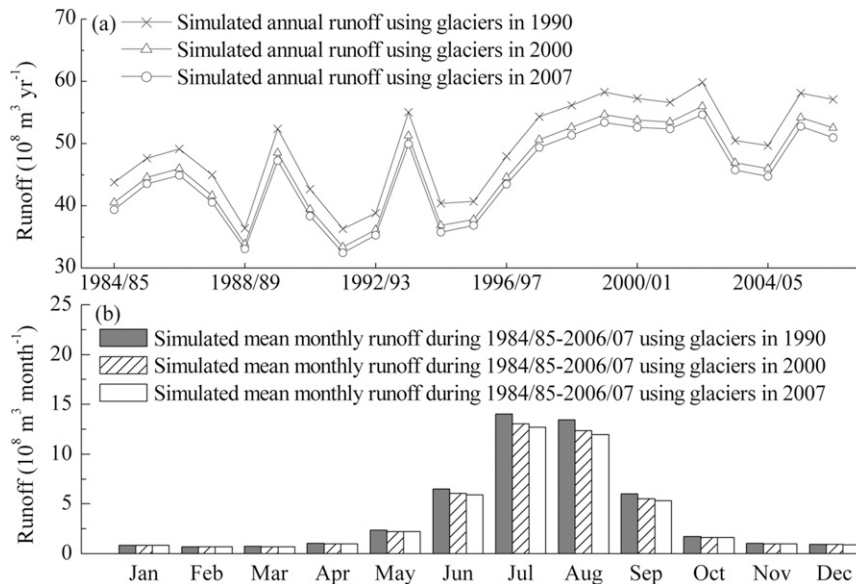


FIG. 8. Simulated (a) annual and (b) mean monthly runoff during 1984/85–2006/07 for glaciers at three periods (1990, 2000, and 2007).

which can be classified into two types. The first type of precipitation product is produced based on gauged observational data, represented by APHRODITE and the Global Precipitation Climatology Centre (GPCC; Rudolf et al. 2010). The second type of product is produced based on satellite and gauged measurements and it is represented by the Global Precipitation Climatology Project (GPCP; Adler et al. 2003). We tried simulating discharge by adopting all three different precipitation products (Fig. 10). Of the three simulations, the simulated runoff using APHRODITE showed best agreement with the observations, as shown in Fig. 10a.

The simulated runoff using APHRODITE, GPCC, and GPCP resulted in underestimations of 11%, 20%, and 14%, respectively. In the Kunma Like River catchment, the simulations using the precipitation products were lower than the observed data because there is only one precipitation gauging station within the alpine region.

We performed sensitivity tests to demonstrate how the uncertainties in precipitation and air temperature affect the runoff simulations in the Kunma Like basin. Figure 11 shows that the simulations are very sensitive to uncertainties in air temperature change. If the input air

TABLE 5. Temperature differences and precipitation ratios between future scenarios (2050s, 2044/45–2053/54) and reference simulation (1984/85–2006/07) under three emission scenarios, averaged over study catchment.

	Jan	Feb	Mar	Apr	May	Jun	Jul	Aug	Sep	Oct	Nov	Dec	Year
RCP2.6 scenario													
ΔT_{avg} ($^{\circ}\text{C}$)	1.56	1.67	1.59	1.76	2.18	2.30	2.55	2.54	2.71	1.74	1.86	1.83	2.02
ΔT_{max} ($^{\circ}\text{C}$)	1.15	1.25	1.58	1.62	1.96	2.09	2.31	2.34	2.96	2.03	1.84	1.59	1.89
ΔT_{min} ($^{\circ}\text{C}$)	1.67	1.95	1.67	1.46	2.14	2.23	2.62	2.57	2.21	1.22	2.03	2.24	2.00
ΔP (%)	0.99	1.04	1.08	1.09	1.07	0.94	1.05	1.13	0.70	0.81	0.98	1.08	1.00
RCP4.5 scenario													
ΔT_{avg} ($^{\circ}\text{C}$)	1.79	2.44	2.03	1.82	2.86	2.67	2.75	3.32	3.14	1.91	1.43	1.91	2.34
ΔT_{max} ($^{\circ}\text{C}$)	1.52	2.08	2.09	1.75	3.02	2.62	2.72	3.55	3.41	2.24	1.69	1.68	2.36
ΔT_{min} ($^{\circ}\text{C}$)	2.15	2.99	2.14	1.87	2.69	2.77	2.89	3.12	2.90	1.57	1.43	2.09	2.38
ΔP (%)	1.00	1.02	1.13	1.19	0.94	1.20	1.17	0.97	1.17	0.88	1.00	0.97	1.05
RCP8.5 scenario													
ΔT_{avg} ($^{\circ}\text{C}$)	2.88	2.80	2.96	2.39	2.40	2.99	3.46	3.87	3.80	3.33	2.62	3.61	3.09
ΔT_{max} ($^{\circ}\text{C}$)	2.02	2.36	3.08	2.56	2.30	2.95	3.52	3.94	4.07	3.86	2.76	3.07	3.04
ΔT_{min} ($^{\circ}\text{C}$)	3.53	3.51	3.19	2.18	2.69	3.22	3.61	4.00	3.67	2.87	2.86	4.19	3.29
ΔP (%)	1.16	1.11	1.12	1.09	1.21	1.13	1.24	1.10	0.88	0.83	0.97	1.08	1.08

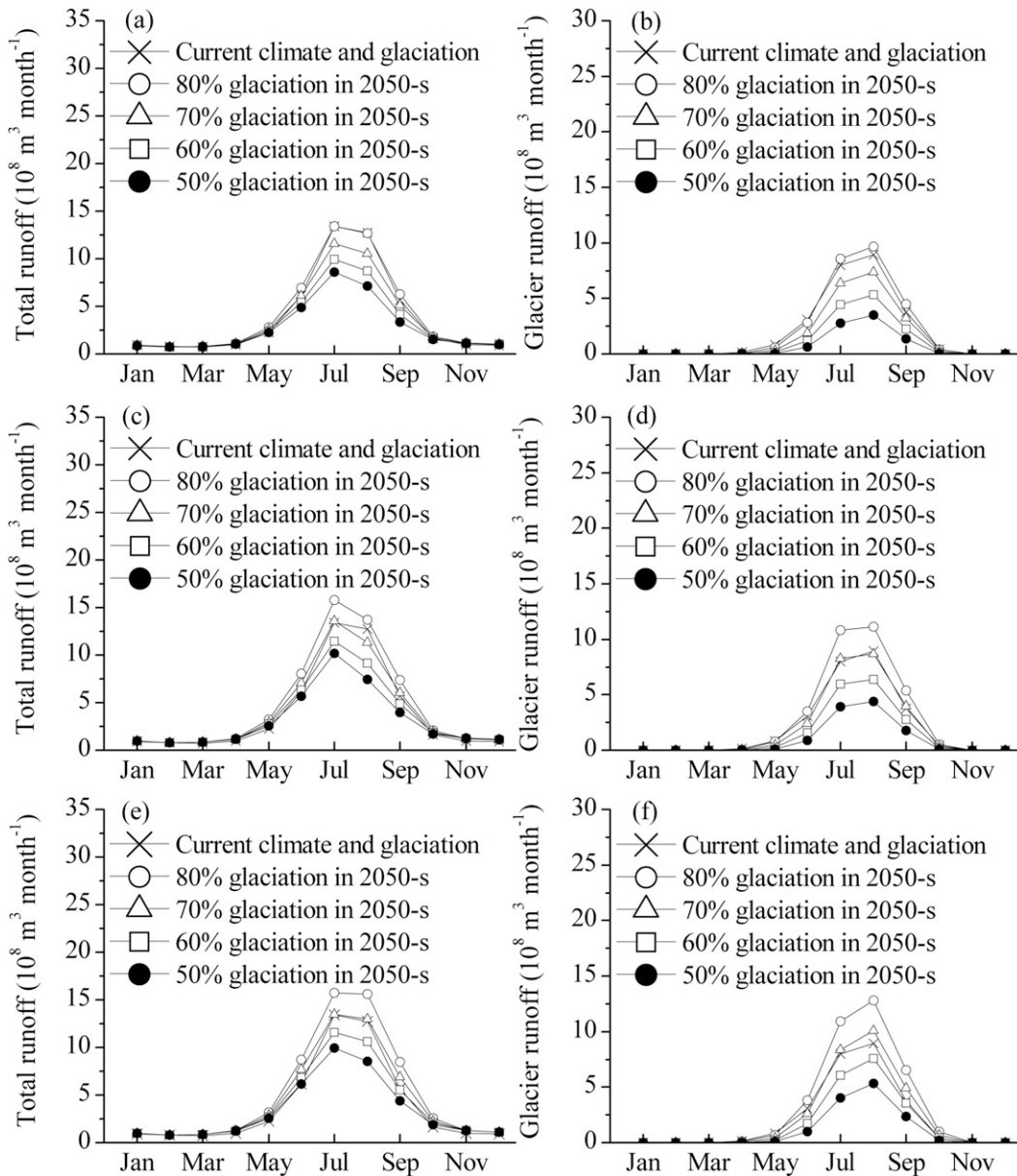


FIG. 9. Simulated mean monthly total river runoff and glacier runoff under present climate and future climate scenarios: (a),(b) RCP2.6; (c),(d) RCP4.5; and (e),(f) RCP8.5 for four glacier coverages (relative to glacier area in 2007) over entire simulation period (23 years).

temperature is 1°C higher or lower than the actual temperature, the glacier runoff, total runoff, and glacier mass balance will be overestimated or underestimated by 34%, 20%, and 57%, respectively. The simulated glacier runoff and mass balance are less sensitive to uncertainties in precipitation. A 10% overestimation or underestimation of input precipitation will result in a 0.2% and 6% underestimation or overestimation in glacier runoff and glacier mass balance, respectively. An increase of precipitation will slightly reduce the level of glacier melting.

A 10% increase or decrease in precipitation will cause a 5% increase or decrease in total runoff.

An accurate spatial distribution of air temperature is more easily obtained than for precipitation because of its greater reliability with elevation, and thus the influence of uncertainty in air temperature on the simulation is smaller. Detailed analyses suggest that uncertainties of simulated glacier runoff, total runoff, and glacier mass balance due to precipitation are about 0.5%, 11%, and 13%, respectively (Figs. 10, 11).

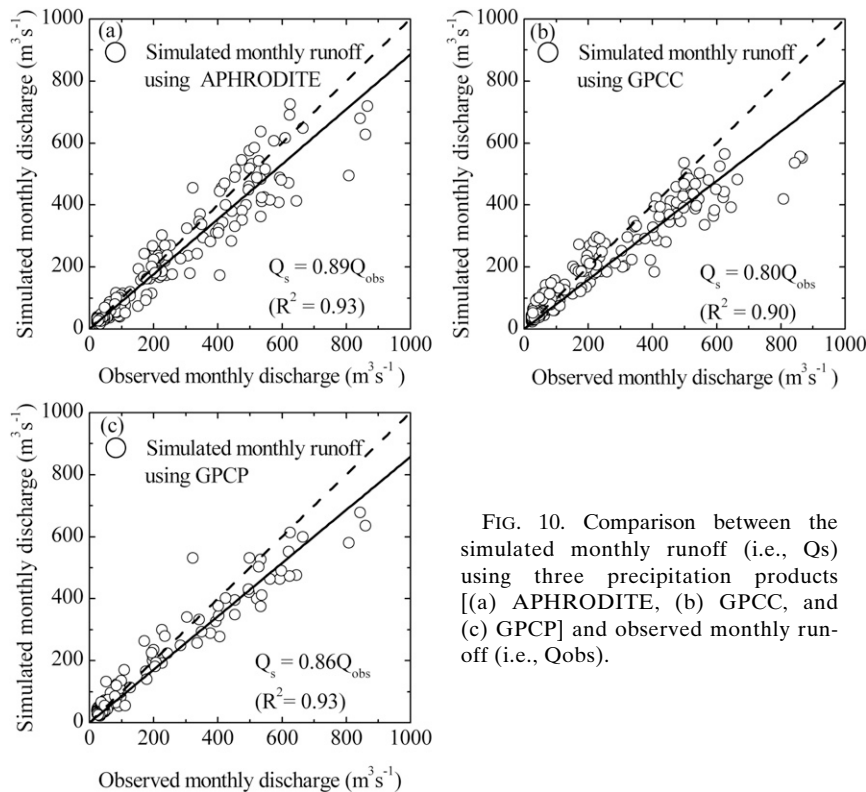


FIG. 10. Comparison between the simulated monthly runoff (i.e., Q_s) using three precipitation products [(a) APHRODITE, (b) GPCC, and (c) GPCP] and observed monthly runoff (i.e., Q_{obs}).

The parameters of the model each have a certain degree of uncertainty. There are most likely temporal dynamics in the D_{snow} and D_{ice} parameters (Cui et al. 2010), and glacier melt is also likely affected by glacier surface debris and black carbon (Ramanathan and Carmichael 2008). Because of insufficient empirical data, it is difficult to quantitatively account for these factors in a semidistributed glacier melt model. When the snow and ice degree-day factors increase or decrease by $1 \text{ mm } ^\circ\text{C}^{-1} \text{ day}^{-1}$, the simulated glacier runoff will increase or decrease by about 20%, based on the degree-day model for calculating the melting of the snow and ice. According to the contribution of glaciers to the total discharge, simulated total runoff will increase or decrease by about 10%. Assuming the degree factors to be Gaussian deviates with standard deviation $\sigma = 1 \text{ mm } ^\circ\text{C}^{-1} \text{ day}^{-1}$ (Immerzeel et al. 2010), the uncertainty of simulating and projecting total runoff from degree-day factors is likely to be about 10%.

6. Conclusions

The glacier area in the Kunma Like River catchment shrank by 415.9 km^2 (13.2%) from 1990 to 2007, or $24.46 \text{ km}^2 \text{ yr}^{-1}$. A degree-day melt model was coupled with the macroscale hydrologic VIC, which considered

the subgrid glacier processes through the establishment of glacier elevation bands. The extended VIC showed acceptable performance for the data-sparse alpine basin.

Annual runoff of the catchment showed an increasing trend at a rate of $4.07 \times 10^8 \text{ m}^3 \text{ decade}^{-1}$, attributable to increasing precipitation and air temperature from 1984/85 to 2006/07. Comparisons indicated that for glacier area losses of 8.9% and 13.2%, annual river discharge decreased by 6.9% and 9.3% and summer runoff decreased by 7.7% and 10.4%, respectively. The shrinkage of glaciers also enhanced interannual variance of discharge.

The simulation suggests that if glaciers were to shrink by $>30\%$, annual discharge would likely decline by the 2050s, because of reduced glacier meltwater. According to the present rate of shrinkage of the glacier area, annual discharge of the Kunma Like River is projected to likely decrease by 2.8%–19.4% under the 2050s scenario, relative to the reference period (1984/85–2006/07).

Acknowledgments. This work was supported by the National Major Scientific Research Program of China (2013CBA01806), Foundation of State Key Laboratory of Cryospheric Science (SKLCS-ZZ-2013-2-1), National Nature Science Foundation of China (NSFC) (41201025, 41130638, 41271090, 41471060, and 41271082), Knowledge

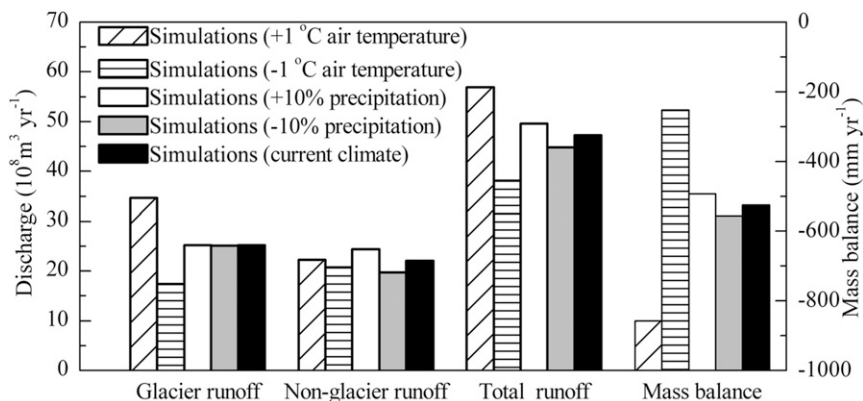


FIG. 11. Annual discharge and glacier mass balance simulations in the Kunma Like River for different meteorological input data (air temperature and precipitation) during 1984/85–2006/07.

Innovation Program of the Chinese Academy of Sciences (KZCX2-YW-GJ04), and the Foundation for Young Talents in Cold and Arid Regions Environmental and Engineering Research Institute of CAS (Y451191001). Our grateful thanks are due to Hubert Savenije for insightful suggestions.

REFERENCES

- Adler, R. F., and Coauthors, 2003: The version 2 Global Precipitation Climatology Project (GPCP) Monthly Precipitation Analysis (1979–present). *J. Hydrometeorol.*, **4**, 1147–1167, doi:[10.1175/1525-7541\(2003\)004<1147:TVGPCP>2.0.CO;2](https://doi.org/10.1175/1525-7541(2003)004<1147:TVGPCP>2.0.CO;2).
- Aizen, V. B., E. M. Aizen, A. B. Surazakov, and V. A. Kuzmichenok, 2006: Assessment of glacial area and volume change in Tien Shan (central Asia) during the last 150 years using geodetic, aerial photo, ASTER and SRTM data. *Ann. Glaciol.*, **43**, 202–213, doi:[10.3189/172756406781812465](https://doi.org/10.3189/172756406781812465).
- Bentsen, M., and Coauthors, 2013: The Norwegian Earth System Model, NorESM1-M—Part 1: Description and basic evaluation of the physical climate. *Geosci. Model Dev.*, **6**, 687–720, doi:[10.5194/gmd-6-687-2013](https://doi.org/10.5194/gmd-6-687-2013).
- Blandford, T. R., K. S. Humes, B. J. Harshburger, B. C. Moore, V. P. Walden, and H. Ye, 2008: Seasonal and synoptic variations in near-surface air temperature lapse rates in a mountainous basin. *J. Appl. Meteor. Climatol.*, **47**, 249–261, doi:[10.1175/2007JAMC1565.1](https://doi.org/10.1175/2007JAMC1565.1).
- Bohn, T. J., B. Livneh, J. W. Oyster, S. W. Running, B. Nijssen, and D. P. Lettenmaier, 2013: Global evaluation of MTCLIM and related algorithms for forcing of ecological and hydrological models. *Agric. For. Meteorol.*, **176**, 38–49, doi:[10.1016/j.agrformet.2013.03.003](https://doi.org/10.1016/j.agrformet.2013.03.003).
- Bolch, T., 2007: Climate change and glacier retreat in northern Tien Shan (Kazakhstan/Kyrgyzstan) using remote sensing data. *Global Planet. Change*, **56**, 1–12, doi:[10.1016/j.gloplacha.2006.07.009](https://doi.org/10.1016/j.gloplacha.2006.07.009).
- Bowling, L. C., J. W. Pomeroy, and D. P. Lettenmaier, 2004: Parameterization of blowing-snow sublimation in a macroscale hydrology model. *J. Hydrometeorol.*, **5**, 745–762, doi:[10.1175/1525-7541\(2004\)005<0745:POBSIA>2.0.CO;2](https://doi.org/10.1175/1525-7541(2004)005<0745:POBSIA>2.0.CO;2).
- Bras, R. A., 1990: *Hydrology: An Introduction to Hydrologic Science*. Addison-Wesley, 643 pp.
- Braun, L. N., M. Weber, and M. Schulz, 2000: Consequences of climate change for runoff from Alpine regions. *Ann. Glaciol.*, **31**, 19–25, doi:[10.3189/172756400781820165](https://doi.org/10.3189/172756400781820165).
- Chen, Y. N., K. Takeuchi, C. C. Xu, Y. P. Chen, and Z. X. Xu, 2006: Regional climate change and its effects on river runoff in the Tarim basin, China. *Hydrol. Processes*, **20**, 2207–2216, doi:[10.1002/hyp.6200](https://doi.org/10.1002/hyp.6200).
- , X. M. Hao, and C. C. Xu, 2007: The trend analysis of runoff change of Tarim River basin, Xin Jiang (in Chinese). *Prog. Nat. Sci.*, **17**, 205–210.
- Cherkauer, K. A., and D. P. Lettenmaier, 1999: Hydrologic effects of frozen soils in the upper Mississippi River basin. *J. Geophys. Res.*, **104**, 19 599–19 610, doi:[10.1029/1999JD900337](https://doi.org/10.1029/1999JD900337).
- , and —, 2003: Simulation of spatial variability in snow and frozen soil. *J. Geophys. Res.*, **108**, 8858, doi:[10.1029/2003JD003575](https://doi.org/10.1029/2003JD003575).
- Costa-Cabral, M. C., J. E. Richey, G. Goteti, D. P. Lettenmaier, C. Feldkötter, and A. Snidvongs, 2008: Landscape structure and use, climate, and water movement in the Mekong River basin. *Hydrol. Processes*, **22**, 1731–1746, doi:[10.1002/hyp.6740](https://doi.org/10.1002/hyp.6740).
- Cui, Y., B. Ye, J. Wang, Y. Liu, and Z. Jing, 2010: Analysis of the spatial-temporal variations of the positive degree-day factors on the glacier No. 1 at the headwaters of the Urümqi River (in Chinese). *J. Glaciol. Geocryology*, **32**, 265–274.
- Donner, L. J., and Coauthors, 2011: The dynamical core, physical parameterizations, and basic simulation characteristics of the atmospheric component AM3 of the GFDL global coupled model CM3. *J. Climate*, **24**, 3484–3519, doi:[10.1175/2011JCLI3955.1](https://doi.org/10.1175/2011JCLI3955.1).
- Farr, T. G., and Coauthors, 2007: The Shuttle Radar Topography Mission. *Rev. Geophys.*, **45**, RG2004, doi:[10.1029/2005RG000183](https://doi.org/10.1029/2005RG000183).
- Fekete, B. M., and C. J. Vorosmarty, 2004: Uncertainties in precipitation and their impacts on runoff estimates. *J. Climate*, **17**, 294–304, doi:[10.1175/1520-0442\(2004\)017<0294:UIPATI>2.0.CO;2](https://doi.org/10.1175/1520-0442(2004)017<0294:UIPATI>2.0.CO;2).
- Gao, H. K., X. B. He, B. S. Ye, and J. C. Pu, 2012: Modeling the runoff and glacier mass balance in a small watershed on the central Tibetan Plateau, China, from 1955 to 2008. *Hydrol. Processes*, **26**, 1593–1603, doi:[10.1002/hyp.8256](https://doi.org/10.1002/hyp.8256).
- Gao, X., B. S. Ye, S. Q. Zhang, C. J. Qiao, and X. W. Zhang, 2010: Glacier runoff variation and its influence on river runoff

- during 1961–2006 in the Tarim River basin, China. *Sci. China Earth Sci.*, **53**, 880–891, doi:10.1007/s11430-010-0073-4.
- Global Soil Data Task Group, 2000: Global gridded surfaces of selected soil characteristics (IGBP-DIS) data set. Oak Ridge National Laboratory Distributed Active Archive Center, accessed 15 October 2013, doi:10.3334/ORNLDAAAC/569.
- Hagg, W., L. N. Braun, M. Kuhn, and T. I. Nesgaard, 2007: Modelling of hydrological response to climate change in glacierized central Asian catchments. *J. Hydrol.*, **332**, 40–53, doi:10.1016/j.jhydrol.2006.06.021.
- , C. Mayer, A. Lambrecht, and A. Helm, 2008: Sub-debris melt rates on southern Inylchek Glacier, central Tian Shan. *Geogr. Ann., Ser. A*, **90**, 55–63, doi:10.1111/j.1468-0459.2008.00333.x.
- Han, H. D., J. Wang, X. Wang, and P. F. Zhang, 2009: Study of the positive degree-day factor of ice cliff ablation in debris-covered area of the Koxkar Glacier (in Chinese). *J. Glaciol. Geocryology*, **31**, 620–627.
- Han, Z. Y., and T. J. Zhou, 2012: Assessing the quality of APHRODITE high-resolution daily precipitation dataset over contiguous China (in Chinese). *Chin. J. Atmos. Sci.*, **36**, 361–373.
- Hansen, M., R. DeFries, J. R. G. Townshend, and R. Sohlberg, 1998: UMD Global Land Cover Classification, 1 kilometer, version 1.0. Department of Geography, University of Maryland, College Park, accessed 10 October, 2013. [Available online at <http://glcf.umd.edu/data/landcover/>.]
- Hock, R., 2003: Temperature index melt modelling in mountain areas. *J. Hydrol.*, **282**, 104–115, doi:10.1016/S0022-1694(03)00257-9.
- , 2005: Glacier melt: A review of processes and their modelling. *Prog. Phys. Geogr.*, **29**, 362–391, doi:10.1191/0309133305pp453ra.
- , and B. Holmgren, 2005: A distributed surface energy-balance model for complex topography and its application to Storglaciaren, Sweden. *J. Glaciol.*, **51**, 25–36, doi:10.3189/172756505781829566.
- , P. Jansson, and L. Braun, 2005: Modelling the response of mountain glacier discharge to climate warming. *Global Change and Mountain Regions*, M. A. Reasoner, Ed., Advances in Global Change Research, Vol. 23, Springer, 243–252, doi:10.1007/1-4020-3508-X_25.
- Hu, Y. J., 2004: *Physical Geography of the Tianshan Mountains in China* (in Chinese). China Environmental Science Press, 443 pp.
- Huang, M. Y., and X. Liang, 2006: On the assessment of the impact of reducing parameters and identification of parameter uncertainties for a hydrologic model with applications to ungauged basins. *J. Hydrol.*, **320**, 37–61, doi:10.1016/j.jhydrol.2005.07.010.
- Huss, M., D. Farinotti, A. Bauder, and M. Funk, 2008: Modelling runoff from highly glacierized alpine drainage basins in a changing climate. *Hydrol. Processes*, **22**, 3888–3902, doi:10.1002/hyp.7055.
- Immerzeel, W. W., L. P. H. Van Beek, and M. F. P. Bierkens, 2010: Climate change will affect the Asian water towers. *Science*, **328**, 1382–1385, doi:10.1126/science.1183188.
- , —, M. Konz, A. B. Shrestha, and M. F. P. Bierkens, 2012: Hydrological response to climate change in a glacierized catchment in the Himalayas. *Climatic Change*, **110**, 721–736, doi:10.1007/s10584-011-0143-4.
- Iversen, T., and Coauthors, 2013: The Norwegian Earth System Model, NorESM1-M—Part 2: Climate response and scenario projections. *Geosci. Model Dev.*, **6**, 389–415, doi:10.5194/gmd-6-389-2013.
- Jiang, X., N. L. Wang, J. Q. He, X. B. Wu, and G. J. Song, 2010: A distributed surface energy and mass balance model and its application to a mountain glacier in China. *Chin. Sci. Bull.*, **55**, 2079–2087, doi:10.1007/s11434-010-3068-9.
- Jiang, Y., C. H. Zhou, and W. M. Cheng, 2005: Analysis on runoff supply and variation characteristics of Aksu drainage basin (in Chinese). *J. Nat. Resour.*, **20**, 27–34.
- Kang, E., G. Cheng, Y. Lan, and H. Jin, 1999: A model for simulating the response of runoff from the mountainous watersheds of inland river basins in the arid area of northwest China to climatic changes. *Sci. China Series D*, **42**, 52–63, doi:10.1007/BF02878853.
- Kattel, D. B., T. Yao, K. Yang, L. Tian, G. Yang, and D. Joswiak, 2013: Temperature lapse rate in complex mountain terrain on the southern slope of the central Himalayas. *Theor. Appl. Climatol.*, **113**, 671–682, doi:10.1007/s00704-012-0816-6.
- Klok, E. J., K. Jasper, K. P. Roelofsma, J. Gurtz, and A. Badoux, 2001: Distributed hydrological modelling of a heavily glaciated Alpine river basin. *Hydrol. Sci. J.*, **46**, 553–570, doi:10.1080/02626660109492850.
- Kotlyakov, V. M., and I. V. Severskiy, 2009: Glaciers of central Asia: Current situation, changes and possible impact on water resources. *Assess. Snow Glacier Water Resour. Asia*, **8**, 36–43.
- Lang, H., 1986: Forecasting meltwater runoff from snow-covered areas and from glacier basins. *River Flow Modelling and Forecasting*, D. A. Kraijenhoff and J. R. Moll, Eds., Water Science and Technology Library, Vol. 3, D. Reidel, 99–127.
- Li, J., S. Y. Liu, H. D. Han, Y. Zhang, J. Wang, and J. F. Wei, 2012: Evaluation of runoff from Koxkar Glacier basin, Tianshan Mountains, China (in Chinese). *Adv. Climate Change Res.*, **8**, 350–356.
- Li, X. Y., 2010: Economical evaluation on the agricultural water-save irrigation technology in arid areas of Xinjiang (in Chinese). M.S. thesis, Xinjiang Agricultural University, 56 pp.
- Liang, X., D. P. Lettenmaier, E. F. Wood, and S. J. Burges, 1994: A simple hydrologically based model of land-surface water and energy fluxes for general-circulation models. *J. Geophys. Res.*, **99**, 14 415–14 428, doi:10.1029/94JD00483.
- , —, and —, 1996: One-dimensional statistical dynamic representation of subgrid spatial variability of precipitation in the two-layer variable infiltration capacity model. *J. Geophys. Res.*, **101**, 21 403–21 422, doi:10.1029/96JD01448.
- Liu, C. H., 1995: Glacier resources and distributive characteristics in the central Asia Tianshan Mountains (in Chinese). *J. Glaciol. Geocryology*, **17**, 193–203.
- Liu, S. Y., Y. J. Ding, and B. S. Ye, 1996: Study on the mass balance of the glacier No.1 at the headwaters of the Urumqi River using degree-day method (in Chinese). *Proceedings of the Fifth Chinese Conference on Glaciology and Geocryology*, Gansu Culture Press, 197–204.
- , W. X. Sun, Y. P. Shen, and G. Li, 2003: Glacier changes since the Little Ice Age maximum in the western Qilian Shan, northwest China, and consequences of glacier runoff for water supply. *J. Glaciol.*, **49**, 117–124, doi:10.3189/172756503781830926.
- , and Coauthors, 2006: Glacier retreat as a result of climate warming and increased precipitation in the Tarim River basin, northwest China. *Ann. Glaciol.*, **43**, 91–96, doi:10.3189/172756406781812168.
- Liu, Y. H., J. M. Feng, and Z. G. Ma, 2014: An analysis of historical and future temperature fluctuations over China based on CMIP5 simulations. *Adv. Atmos. Sci.*, **31**, 457–467, doi:10.1007/s00376-013-3093-0.

- Lohmann, D., E. Raschke, B. Nijssen, and D. P. Lettenmaier, 1998a: Regional scale hydrology: I. Formulation of the VIC-2L model coupled to a routing model. *Hydrol. Sci. J.*, **43**, 131–141, doi:10.1080/02626669809492107.
- , —, —, and —, 1998b: Regional scale hydrology: II. Application of the VIC-2L model to the Weser River, Germany. *Hydrol. Sci. J.*, **43**, 143–158, doi:10.1080/02626669809492108.
- Malone, E. L., 2010: Changing glaciers and hydrology in Asia: Addressing vulnerabilities to glacier melt impacts. USAID Doc., United States Agency for International Development, 119 pp. [Available online at http://pdf.usaid.gov/pdf_docs/Pnadu628.pdf.]
- Meinshausen, M., and Coauthors, 2011: The RCP greenhouse gas concentrations and their extensions from 1765 to 2300. *Climatic Change*, **109**, 213–241, doi:10.1007/s10584-011-0156-z.
- Mokhov, I. I., and M. G. Akperov, 2006: Tropospheric lapse rate and its relation to surface temperature from reanalysis data. *Izv., Atmos. Ocean. Phys.*, **42**, 430–438, doi:10.1134/S0001433806040037.
- Nakawo, M., and B. Rana, 1999: Estimate of ablation rate of glacier ice under a supraglacial debris layer. *Geogr. Ann., Ser. A*, **81**, 695–701, doi:10.1111/j.0435-3676.1999.00097.x.
- Narama, C., A. Kaab, M. Duishonakunov, and K. Abdrakhmatov, 2010: Spatial variability of recent glacier area changes in the Tien Shan Mountains, central Asia, using Corona (similar to 1970), Landsat (similar to 2000), and ALOS (similar to 2007) satellite data. *Global Planet. Change*, **71**, 42–54, doi:10.1016/j.gloplacha.2009.08.002.
- Nash, J. E., and J. V. Sutcliffe, 1970: River flow forecasting through conceptual models. Part I: A discussion of principles. *J. Hydrol.*, **10**, 282–290, doi:10.1016/0022-1694(70)90255-6.
- Nijssen, B., R. Schnur, and D. P. Lettenmaier, 2001: Global retrospective estimation of soil moisture using the Variable Infiltration Capacity land surface model, 1980–93. *J. Climate*, **14**, 1790–1808, doi:10.1175/1520-0442(2001)014<1790:GREOSM>2.0.CO;2.
- Østrem, G., 1959: Ice melting under a thin layer of moraine, and the existence of ice cores in moraine ridges. *Geogr. Ann.*, **41**, 228–230.
- Piao, S. L., and Coauthors, 2010: The impacts of climate change on water resources and agriculture in China. *Nature*, **467**, 43–51, doi:10.1038/nature09364.
- Pieczonka, T., T. Bolch, W. Junfeng, and S. Y. Liu, 2013: Heterogeneous mass loss of glaciers in the Aksu–Tarim catchment (Central Tien Shan) revealed by 1976 KH-9 Hexagon and 2009 SPOT-5 stereo imagery. *Remote Sens. Environ.*, **130**, 233–244, doi:10.1016/j.rse.2012.11.020.
- Pielke, S. R., and R. L. Wilby, 2012: Regional climate downscaling: What's the point? *Eos, Trans. Amer. Geophys. Union*, **93**, 52–53, doi:10.1029/2012EO050008.
- Popovnin, V. V., and A. V. Rozova, 2002: Influence of sub-debris thawing on ablation and runoff of the Djankuat Glacier in the Caucasus. *Nord. Hydrol.*, **33**, 75–94.
- Ramanathan, V., and G. Carmaichael, 2008: Global and regional climate changes due to black carbon. *Nat. Geosci.*, **1**, 221–227, doi:10.1038/ngeo156.
- Rudolf, B., B. Andreas, S. Udo, M. C. Anja, and Z. Markus, 2010: The new “GPCC Full Data Reanalysis Version 5” providing high-quality gridded monthly precipitation data for the global land-surface is public available since December 2010. GPCC Status Rep., GPCC, 7 pp.
- Schaeffli, B., and M. Huss, 2011: Integrating point glacier mass balance observations into hydrologic model identification. *Hydrol. Earth Syst. Sci.*, **15**, 1227–1241, doi:10.5194/hess-15-1227-2011.
- Shangguan, D., S. Y. Liu, Y. J. Ding, L. F. Ding, J. L. Xu, and L. Jing, 2009: Glacier changes during the last forty years in the Tarim Interior River basin, northwest China. *Prog. Nat. Sci.*, **19**, 727–732, doi:10.1016/j.pnsc.2008.11.002.
- Shen, Y. P., G. Y. Wang, Y. J. Ding, W. Y. Mao, S. Y. Liu, S. D. Wang, and D. M. Mamatkanov, 2009: Changes in glacier mass balance in watershed of Sary Jaz-Kumarik rivers of Tianshan Mountains in 1957–2006 and their impact on water resources and trend to end of the 21st century (in Chinese). *J. Glaciol. Geocryology*, **31**, 792–800.
- Shi, Y. F., 2008: *Glaciers and Related Environments in China* (in Chinese). Science Press, 539 pp.
- , Y. P. Shen, and R. J. Hu, 2002: Preliminary study on signal, impact and foreground of climatic shift from warm–dry to warm–humid in northwest China (in Chinese). *J. Glaciol. Geocryology*, **24**, 219–226.
- Singh, P., and N. Kumar, 1997: Impact assessment of climate change on the hydrological response of a snow and glacier melt runoff dominated Himalayan river. *J. Hydrol.*, **193**, 316–350, doi:10.1016/S0022-1694(96)03142-3.
- Singh, M. P., P. Singh, and U. K. Haritashya, 2011: *Encyclopedia of Snow, Ice and Glaciers*. Springer, 1300 pp.
- Sorg, A., T. Bolch, M. Stoffel, O. Solomina, and M. Beniston, 2012: Climate change impacts on glaciers and runoff in Tien Shan (central Asia). *Nat. Climate Change*, **2**, 725–731, doi:10.1038/nclimate1592.
- Tang, Q. C., Y. G. Qu, and Y. M. Zhou, 1992: *Hydrology and Water Resources of Arid Area in China* (in Chinese). Science Press, 195 pp.
- Thornton, P. E., and S. W. Running, 1999: An improved algorithm for estimating incident daily solar radiation from measurements of temperature, humidity, and precipitation. *Agric. For. Meteorol.*, **93**, 211–228, doi:10.1016/S0168-1923(98)00126-9.
- UNDP, 2009: Second national communication of the Kyrgyz Republic to the United Nations Framework Convention on Climate Change. UNDP, 199 pp.
- Wang, S. J., M. J. Zhang, Z. Q. Li, F. T. Wang, H. L. Li, Y. J. Li, and X. Y. Huang, 2011: Glacier area variation and climate change in the Chinese Tianshan Mountains since 1960. *J. Geogr. Sci.*, **21**, 263–273, doi:10.1007/s11442-011-0843-8.
- Webb, R. S., C. E. Rosenzweig, and E. R. Levine, 1993: Specifying land surface characteristics in general circulation models: Soil profile data set and derived water-holding capacities. *Global Biogeochem. Cycles*, **7**, 97–108, doi:10.1029/92GB01822.
- Wei, F. F., J. P. Tang, and P. H. Hui, 2013: Comparing high-resolution rain gauge–based precipitation data with satellite rainfall estimates of TRMM 3B42 over Asia. *J. Nanjing Univ.*, **49**, 320–330.
- Xie, Z. H., and F. Yuan, 2006: A parameter estimation scheme of the land surface model VIC using the MOPEX databases. *IAHS Publ.*, **307**, 169–179.
- Xu, J. L., S. Y. Liu, S. Q. Zhang, W. Q. Guo, and J. Wang, 2013: Recent changes in glacial area and volume on Tuanjiefeng Peak region of Qilian Mountains, China. *PLoS One*, **8**, e70574, doi:10.1371/journal.pone.0070574.
- Yatagai, A., K. Kamiguchi, O. Arakawa, A. Hamada, N. Yasutomi, and A. Kitoh, 2012: APHRODITE constructing a long-term daily gridded precipitation dataset for Asia based on a dense network of rain gauges. *Bull. Amer. Meteor. Soc.*, **93**, 1401–1415, doi:10.1175/BAMS-D-11-00122.1.

- Ye, B. S., Y. J. Ding, K. Q. Jiao, Y. P. Shen, and J. Zhang, 2012: The response of river discharge to climate warming in cold region over China (in Chinese). *Quat. Sci.*, **32**, 103–110.
- Yu, P. J., H. L. Xu, S. W. Liu, H. Y. An, Q. Q. Zhang, and J. J. Gong, 2011: The nonlinear characteristics of annual runoff change in Aksu River (in Chinese). *J. Nat. Resour.*, **26**, 1412–1422.
- Zemp, M., and Coauthors, 2013: Reanalysing glacier mass balance measurement series. *Cryosphere*, **7**, 1227–1245, doi:[10.5194/tc-7-1227-2013](https://doi.org/10.5194/tc-7-1227-2013).
- Zhang, S. Q., B. S. Ye, S. Y. Liu, X. W. Zhang, and S. Hagemann, 2012a: A modified monthly degree-day model for evaluating glacier runoff changes in China. Part I: Model development. *Hydrol. Processes*, **26**, 1686–1696, doi:[10.1002/hyp.8286](https://doi.org/10.1002/hyp.8286).
- , X. Gao, B. S. Ye, X. W. Zhang, and S. Hagemann, 2012b: A modified monthly degree-day model for evaluating glacier runoff changes in China. Part II: Application. *Hydrol. Processes*, **26**, 1697–1706, doi:[10.1002/hyp.8291](https://doi.org/10.1002/hyp.8291).
- Zhang, Y., S. Y. Liu, D. H. Shangguan, H. D. Han, C. W. Xie, and J. Wang, 2005: Study of the positive degree-day factors on the Koxkar Baqi Glacier on the south slope of Tianshan Mountains (in Chinese). *J. Glaciol. Geocryology*, **27**, 337–343.
- , —, C. W. Xie, and Y. J. Ding, 2006: Application of a degree-day model for the determination of contributions to glacier meltwater and runoff near Keqicar Baqi Glacier, southwestern Tien Shan. *Ann. Glaciol.*, **43**, 280–284, doi:[10.3189/172756406781812320](https://doi.org/10.3189/172756406781812320).
- Zhao, Q. D., B. S. Ye, Y. J. Ding, S. Q. Zhang, C. C. Zhao, J. Wang, and Z. R. Wang, 2011: Simulation and analysis of river runoff in typical cold regions. *Sci. Cold Arid Reg.*, **3**, 498–508.
- , and Coauthors, 2013: Coupling a glacier melt model to the Variable Infiltration Capacity (VIC) model for hydrological modeling in north-western China. *Environ. Earth Sci.*, **68**, 87–101, doi:[10.1007/s12665-012-1718-8](https://doi.org/10.1007/s12665-012-1718-8).